Journal Pre-proof

Numerical analysis of wind-induced natural ventilation for an isolated cubic room with two openings under small mean wind pressure difference

Tomohiro Kobayashi, Mats Sandberg, Takuya Fujita, Eunsu Lim, Noriko Umemiya

Please cite this article as: Kobayashi T, Sandberg M, Fujita T, Lim E, Umemiya N, Numerical analysis of wind-induced natural ventilation for an isolated cubic room with two openings under small mean wind pressure difference, *Building and Environment* (2022), doi: https://doi.org/10.1016/j.buildenv.2022.109694.

Numerical analysis of wind-induced natural ventilation for an isolated cubic room with two openings under small mean wind pressure difference

Tomohiro Kobayashi [a], Mats Sandberg [b], Takuya Fujita [c], Eunsu Lim [d], Noriko Umemiya [c]

[a] *Division of Global Architecture, Graduate School of Engineering, Osaka University, Osaka, Japan*

[b] *Department of Building Engineering, Energy Systems and Sustainability Science, University of Gävle, Gävle, Sweden*

[c] *Department of Architecture, Graduate School of Engineering, Osaka City University, Osaka, Japan*

[d] *Department of Architecture, Faculty of Science and Engineering, Toyo University, Saitama, Japan*

Abstract

Wind-induced natural ventilation through openings with small wind pressure differences was examined using large eddy simulation (LES) modelling. This study focused on cases in which the ventilation rate is predicted using a standard Orifice equation. The purpose of this study was to clarify how the ventilation rate is underestimated in such cases for both single-sided and double-sided openings, and to clarify the difference between the effective ventilation rate (purging flow rate, PFR) and bulk airflow rate (AFR), which have not been sufficiently and systematically understood. A simple cubic-room model with two openings was analysed using LES by varying the opening position after validation, and the ventilation rate, velocity field, and wind pressure coefficient were compared with experimental results. The PFR was determined by tracing particles, and the AFR was obtained based on the instantaneous velocity over the openings. The AFR predicted by the Orifice equation was underestimated when the difference in the mean wind pressure coefficient ($\Delta \overline{C_p}$) was less than 0.1. The main feature of this study was to show the ventilation effectiveness defined by the PFR divided by AFR, which was approximately 70-80%, 60%, and 90% for the double-sided openings, single-sided openings on the lateral side, and windward and leeward sides, respectively. Another feature was to propose a method for estimating the AFR reflecting two key phenomena, namely pulsating flow and eddy penetration. In addition, a simple equation considering the standard deviation of wind pressure coefficient difference ($\sigma_{\Delta Cp}$), and external local velocity around an opening (V_{vic}) was obtained.

1. Introduction

Natural ventilation can be effective in controlling indoor environments without consuming non-renewable energy[1–7]. It is generally known that natural ventilation is driven by wind, buoyancy, or a combination of the two. Buoyancy-driven ventilation provides a relatively stable airflow and corresponding control of the indoor environment because its pressure difference is caused by the temperature difference. However, it is not always possible to achieve sufficient ventilation using buoyancy-driven ventilation. It can be difficult to obtain sufficiently large openings with sufficiently large height differences. In such cases, the wind pressure difference may be the dominant driving force. When the wind pressure difference between openings is large, a large amount of outdoor air is expected to pass through a building, which is beneficial not only to maintain desirable indoor air quality but also to obtain thermal comfort under moderate climate conditions. This type of wind-induced ventilation is often referred to as cross-ventilation, and much academic attention has been paid to it by means of both wind tunnel measurements and computational fluid dynamics (CFD). Some studies have focused on a single-zone room model and performed wind tunnel tests and CFD predictions to obtain more details on the flow patterns or distributions of wind velocity, pressure, and turbulent statistics[8–12]. The effect of surrounding buildings on cross-ventilation flow has also been investigated[13–16]. Other studies have focused in more detailed on the airflow of a building equipped with some architectural devices which affect cross-ventilation flow such as louvers, monitor roofs, and wind catchers [17–19]. Another study focused on discrepancies between on-site and wind tunnel cases

and performed large eddy simulation (LES) modelling[20]. Owing to its complexity, wind-induced natural ventilation flow has been of great interest over the last several decades.

The rate of natural ventilation is generally predicted using the standard Orifice equation:[21]. When wind is the only driving force, it can be estimated using Eq.(1) for the case of two openings.

$$Q = (C_d A_W)_{connected} V_{ref} \sqrt{\Delta C_P} \qquad (1)$$

where ΔC_P is the difference in the wind pressure coefficient between two openings, obtained from a sealed building model, and usually regarded as a time-averaged value ($\overline{\Delta C_p}$). V_{ref} is the reference velocity of the approaching flow, and its dynamic pressure is used to define the wind pressure coefficients. $(C_d A_W)_{connected}$ is the connected value of the effective opening area of the openings, and it can be represented by the following equation:

$$(C_d A_W)_{connected} = \frac{1}{\sqrt{\frac{1}{(C_{d1} A_{w1})^2} + \frac{1}{(C_{d2} A_{w2})^2}}} \qquad (2)$$

where C_d and A_W are the discharge coefficient and area of each opening, respectively, and the product is interpreted as the effective opening area. Although this classical pressure-based approach has been widely used for the airflow network models[22], it is well known that the Orifice equation includes a number of assumptions that limit its application to practical airflow calculations[23,24]. In cases where the openings are relatively large and the kinetic energy is not sufficiently dissipated after passing through an opening, the Orifice equation is not suitable, and the flow rate may be underestimated[25,26]. Many studies have addressed this issue. Based on the concept of energy balance[27], the power balance model was proposed[28–30] and was followed by studies analysing stream tubes[31,32]. Another study regarded this as a "catchment" problem and demonstrated the necessity of an alternative prediction method to the conventional equation[33]. Apart from the large-opening cases, there also exists the problem of overestimating the flow rate when the angle of external flow incidence to an opening is large. To address this problem, some calculation models have been proposed to modify the discharge coefficients by considering the local similarity[34–38] or vector composition[39,40].

Predicting the wind-induced ventilation rate for single-sided ventilation is also problematic. In buildings in urban areas, it is not always easy to expect cross-ventilation by providing openings on opposite sides because of restrictions related to building plans, fire codes, security requirements, etc. In such cases, single-sided ventilation can be an effective strategy for natural ventilation, although the expected flow rate is less than that of cross-ventilation[41]. When the room is ventilated through only one opening (also referred to as "SS1" [42–44]), Eq.(1) cannot be applied. A number of studies have been performed to estimate the flow rate and to understand the phenomena in detail, as reviewed by Zhong et al.[44]. The air exchange mechanism is classified into four factors: (1) airflow through a compartment, (2) pulsating flow, (3) penetration of eddies (turbulence), and (4) molecular diffusion[45]. Airflow through a compartment explains the ventilation through openings located at different positions and exposed to different pressures, which is similar to forced ventilation. The process of molecular diffusion is slow, and its effect on the flow rate is almost negligible compared to other factors. Consequently, pulsation and eddy penetration are two important factors to be considered for single-sided ventilation with one opening. Cockroft and Robertson [46] obtained a simple theoretical model by focusing on the pulsating flow produced mainly by the low-frequency fluctuating velocity and compressibility of the air. Haghighat et al. [47,48] also focused on pulsating flow and proposed an approach based on a power spectrum analysis. Regarding eddy penetration, Warren [49] assumed a flow pattern, including the mixing layer, and derived a simple formula to estimate the wind-induced ventilation rate, which was followed by studies investigating details focusing on the mixing layer[43,50–53]. Several studies have been performed for the single opening (SS1) case, whose approach involves empirical models, wind tunnel tests, and LES simulations [54–61].

In the case of single-sided ventilation with two openings (referred to as SS2 [42–44]), the inflow/outflow opening alternate periodically when the mean pressure difference is almost negligible[44,45]. In such cases, taking the mean value of ΔC_p in Eq.(1) results in a relatively small prediction result for the ventilation rate, which leads to a considerable underestimation because ventilation can actually be driven by the instantaneous pressure difference between openings. Fundamental studies have also been conducted on this issue. Chu et al. [62] experimentally investigated the ventilation rate and the effects of wind direction. Daish et al. [42] performed wind tunnel tests for two openings on the same external wall and changed the distance between the openings. They also proposed a simple modification of the Orifice equation by introducing the standard deviation of the wind pressure coefficient difference ($\sigma_{\Delta C_p}$) and derived empirical values for the two model coefficients. Arinami et al. [19] conducted LES for single-sided ventilation with two openings to evaluate the performance of guide vanes. The airflow through two openings on the leeward side of an isolated building with single-sided ventilation has attracted academic attention as a form of ventilation where vortex shedding can be a driving force[63]. This type of ventilation was termed "pumping ventilation", and has been investigated in recent studies[64–66]. Jiang et al. [67] also performed a wind tunnel experiment for the cases including SS2 to show that the conventional Orifice equation fails to predict the flow rate under a small wind pressure difference, and they proposed an empirical equation.

Compared with the single-opening case (SS1), there have been few detailed studies on two openings on the same wall (SS2). Therefore, this study explored with the wind-induced natural ventilation of a room equipped with two openings, where the Orifice equation is unsuitable. Depending on the external wind direction, pulsating ventilation with alternating inflow/outflow at an opening can also occur when two openings are provided for perpendicular facades (corner-ventilation, CR2 [66]), or opposite facades (two-sided or lateral openings [14,55]) as well as single-sided ventilation with two openings (SS2). Although the opening arrangement in architectural planning is different among these cases, the phenomenon is similar and the mechanism of ventilation is the same, that is, the mean wind pressure difference is small, and turbulent eddy penetration and pulsating flow are two influencing factors. Therefore, focusing on the situation of a small wind pressure difference, this study analyses a simple rectangular model with two openings for both single-sided and double-sided cases, and had the following research objectives.

· Clarifying how the standard Orifice equation underestimates the flow rate when the mean wind pressure coefficient difference ($\Delta \overline{C_p}$) is small
· Understanding the differences in the ventilation rate tendency between single- and double-sided openings
· Providing information regarding the ratio of the effective ventilation rate to the bulk airflow rate for such cases
· Proposing a simple equation modifying the Orifice equation considering both pulsating flow and eddy penetration

In the present study, wind tunnel tests were first conducted to obtain the wind pressure coefficient and airflow velocity using a sealed model of a simple shape, and the effective ventilation rate was measured using tracer-gas method for a room model with the same configuration equipped with openings. The main aim of this study was to clarify the tendencies of the ratio of the effective flow rate to bulk flow rate to determine ventilation effectiveness, which has not been sufficiently understood for wind-induced natural ventilation to date. Given this aim, numerical simulation is beneficial because the variation of the instantaneous velocity over an opening used to obtain the bulk airflow rate cannot be precisely evaluated experimentally. Therefore, the experimental results were used to validate CFD. Because the target of this study was the flow field including both eddy penetration and pulsating ventilation with alternating inflow/outflow, the Reynolds-averaged Navier–Stokes (RANS) approach was unsuitable, and instantaneous velocity had to be assessed using LES. Thus, LES simulations were performed for several cases of single- and double-sided openings, and both bulk and effective ventilation rates were evaluated to achieve the research objectives. A simple equation for estimating the airflow rate was finally derived by using the wind pressure fluctuation and external velocity around the opening as parameters that reflect the effects of two key phenomena: the pulsating flow and eddy penetration.

2. Wind Tunnel Measurement

2.1. Purpose and outline of wind tunnel experiment

To validate the numerical analysis using the LES shown in the following section, a wind tunnel test was conducted. Two types of measurements were performed, namely measurements of the flow rate and wind pressure coefficient (Cp value). For the former, a test model provided with two openings was used by adopting the tracer-gas method, whereas for the latter, a sealed model was used, where pressure taps were provided without any openings. Because LES calculations were performed for the model both with and without openings, the measured flow rate and Cp value distribution were compared with the numerical results. For CFD validation, the velocity distribution around the sealed model was also measured to determine the accuracy of the flow pattern for the sealed model.

An open-circuit wind tunnel at Osaka City University was used for the measurement, and its cross-section was 1.2 m high and 1.5 m wide. A cubic single-room 1:20 scale model was used with a length, depth, and height of 200 mm. The wind tunnel was equipped with lattice and roughness blocks, and the test model was exposed to a boundary-layer flow (Fig.1 (1) and (2)). The approaching boundary layer flow was set at 10 m/s using a pitot tube installed at a height of 800 mm from the floor of the test section. Fig. 1 (3) shows the vertical profile of the approaching flow measured without the test model, which was obtained using an I-type hotwire anemometer with a 1.0 Hz sampling frequency for 60 s for each height. Here, the velocity was normalised to that measured at 800 mm. Focusing on the range of the height where the model exists, the boundary layer followed the 1/3.5 power law. The streamwise velocity at the building height was 6.73 m/s, and the Reynolds number of the approaching flow was 90,000. Regarding the Reynolds number independence inside the room, the Re based on the opening width and approaching flow velocity at the height of the opening central position (5.52 m/s) was more than 14,000. These conditions were not significantly different from those in similar studies on pumping ventilation, and were sufficiently higher than the recommended value required to meet similarity under isothermal conditions with a bluff body [65]. Therefore, the flow feature of this scaled test was interpreted as similar to that of a full-scale phenomenon.
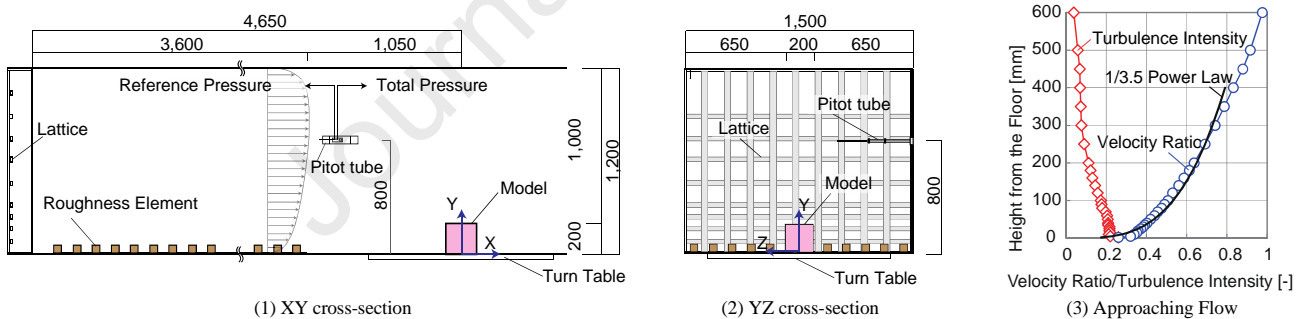

(1) XY cross-section   (2) YZ cross-section   (3) Approaching Flow

Fig. 1. Cross-section of the wind tunnel (dimensions in mm), and profile of the approaching flow

2.2. Flow rate measured using tracer-gas method

To obtain the experimental results of the ventilation rate which were to be compared with CFD, a tracer-gas technique was adopted. A rectangular room model made of a 2.0 mm-thick acrylic board was used, which was equipped with two openings with a side length of 40 mm each. The position of the opening was changed to vary the wind pressure difference between the two openings, and three cases of double-sided openings were studied (Fig. 2). The position of the opening on the right-hand side viewed from the windward side (Opening 2) was varied to change the wind pressure difference, whereas the other opening (Opening 1) was fixed. The intention of the case setting was that Case 2 was the most basic case with a symmetric opening arrangement. In Case 1, Opening 2 was shifted to the windward side exposed to a stronger negative wind pressure, while in Case 3, the opening was moved to the leeward side within a weaker negative pressure.
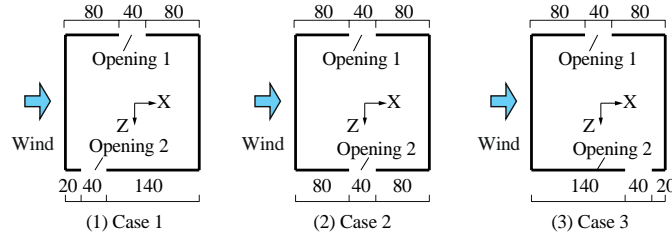
Fig. 2. Studied cases in the wind tunnel experiment (dimensions in mm)

Generally, flow rates can be measured using two types of measurements. One was obtained by integrating the velocity component normal to the opening and expresses the bulk airflow rate. However, this is not always the complete flow rate, that is, it may remove and dilute contaminants. One example is when the flow rate contains a fraction of contaminants that removed. In this study, the bulk airflow rate is referred to as the air flow rate (AFR). The other is defined based on concentration and can be regarded as the effective ventilation rate acting to purge contaminants within a room, referred to as the purging flow rate (PFR), [68] and was used to clarify the difference. Because it is difficult to evaluate the AFR accurately by integrating the velocity over an opening where the inflow and outflow alternates, the PFR, which can be obtained using the tracer-gas concentration, was measured. CO_2 was used as the tracer gas adopted and was supplied from a cylinder (Fig.3 (1)). The tracer gas was injected into the model at the top of the four tubes with a height of 50 mm, and the air inside the room model was sampled through the tube located at the centre of the model to measure the indoor tracer gas concentration (Fig.3 (2) and (3)). Here, the sampling tube was equipped with four small holes at each of the three heights (50, 100, and 150 mm), with the tube top sealed. Therefore, 12 holes were created in total. The reason for this sampling hole arrangement was to measure the average gas concentration as many times as possible within a room where variation in the distribution seemed to exist.
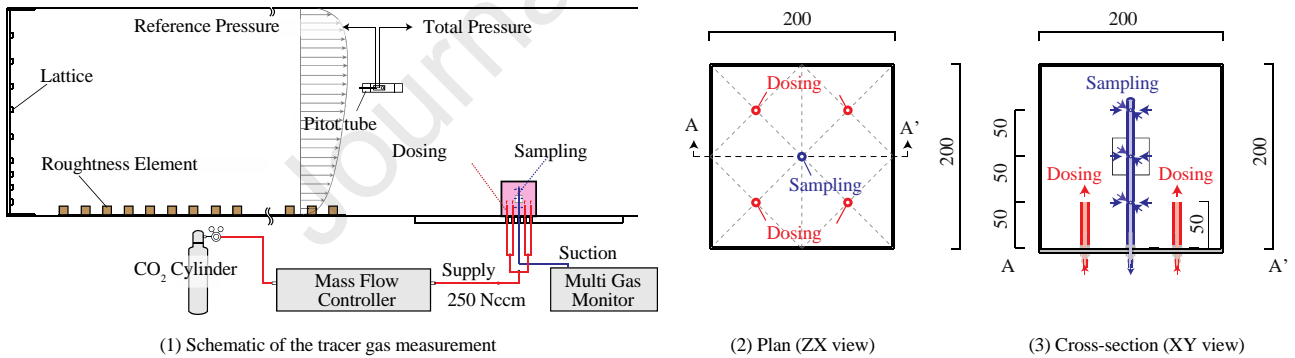

Fig. 3. Experimental setup and dosing/sampling points in the test model (dimensions in mm)

Because the open-circuit wind tunnel was used for the experiment, where the tracer gas never returned to the windward side, the average concentration method of continuous dose methods [69] was applied, and the tracer gas was continuously injected with an emission rate of 250 Nccm using a mass flow controller (Fujikin, FCST1005LC) with a nominal accuracy of ± 10 Nccm. The CO_2 concentration inside the test model was measured by using a gas analyser (LumaSense Technologies, Innova 1312), which was calibrated immediately before the measurement, and the measurement error was confirmed to be 0.32% at a span gas of 5,063 ppm. The concentration was recorded at sampling intervals of 1 minute, and PFR, representing the effective ventilation rate, was calculated using the following equation:

$$PFR = \frac{m}{c_r - c_o} \qquad (3)$$

where m denotes the emission rate of the tracer gas. C_r and C_o are the steady-state indoor and outdoor concentrations, respectively. For the experimental procedure, the CO_2 concentration was measured for 6 min without the tracer gas emission. This was to obtain the background outdoor CO_2 concentration, and the averaged value over this duration was used as the steady-state concentration, C_o. The tracer gas emission then started, and the CO_2 concentration inside the model was continuously measured for 11 min, with the result of the first 1 min discarded. By averaging the concentrations recorded during the remaining 10 min, the steady-state indoor concentration, C_r, was obtained to calculate the PFR. Tracer gas measurement was performed after confirming no significant difference in the results by repeating the preliminary experiment targeted for Case 2 three times.

2.3. Measurement of the wind pressure coefficient and velocity around the sealed building model

Being basic information required for analysing flow rate, the distribution of the time-averaged value of the wind pressure coefficient ($\overline{C_p}$) was evaluated. A sealed model was used to measure $\overline{C_p}$, the configuration of which was the same as that provided with the openings presented in the previous section. Given the symmetry of the model at Z=0, three of the four walls were equipped with pressure taps, and the static pressure on the wall surface was measured as the wind pressure at 19 points on each of the three walls, that is 57 pressure taps were provided in total. Fig. 4 (1) and (2) depict the test model for the wind pressure measurement, showing the position of the pressure taps. All pressure taps were located at a height of 100 mm from the floor, which was the height of the central position of the openings in all the cases studied in the present study. The wind pressure coefficients were measured using a differential pressure transducer (DP-45, Validyne) with a measurement range of ± 220 Pa and nominal accuracy of 0.5% of F.S. The pressure transducer used in this study was calibrated before the measurement using a bell-type manometer (ISP-350, Shibata), with absolute calibration made possible using a weight, and that the RMSE value obtained from 32 measurements of the dynamic pressure of a free flow was less than 0.4 Pa, which was calculated at a pressure of approximately ± 80 Pa and intervals of approximately 5.0 Pa. Because the experiment mainly aimed to measure the mean wind pressure coefficient, $\overline{C_p}$, all the pressure taps were connected to a differential pressure transducer via a switching valve. The other side of the pressure transducer was connected to the static pressure tube of the pitot tube, which was adopted as the reference pressure throughout the experiment. Thus, $\overline{C_p}$ was obtained at each of the 57 points to evaluate its distribution. The measurement was repeated twice, and their average was adopted as the final result, although no significant difference was seen, with a 3.25 % of relative error on average over the 57 points. The difference in $\overline{C_p}$ between the two openings ($\Delta\overline{C_p}$), which is generally regarded as the driving force in the Orifice equation, is discussed.

In addition to the pressure measurement, the velocity profile around the sealed room model was measured to compare the results between the measurement and LES, as presented in the following section. All the measurement points were set at a height of 100 mm from the floor for both the right- and left-hand sides of the model. For each side, 110 measurement points of 10 × 11 were set with intervals of 10 mm in the Z direction and 20 mm in the X direction (Fig. 3 (3) and (4)). An I-type hotwire probe of a 5-μm-diameter tungsten wire (Model 0251R-T5, KANOMAX Japan) was used for the measurement with a sampling frequency of 1.0 kHz, and the velocity was recorded for 60 s to evaluate the average value for each measurement point. The probe was set with its wire parallel to the Z axis (perpendicular to the side wall of the model) and shifted using a traversing unit. After calibrating the hot-wire anemometer by comparing the mean velocity of the free flow with that obtained from a pitot tube, whose dynamic pressure was measured using the above-mentioned pressure transducer, the velocity profile was measured once. The results are presented and discussed later along with those of on the CFD in the following section to determine the accuracy of CFD for the sealed model.
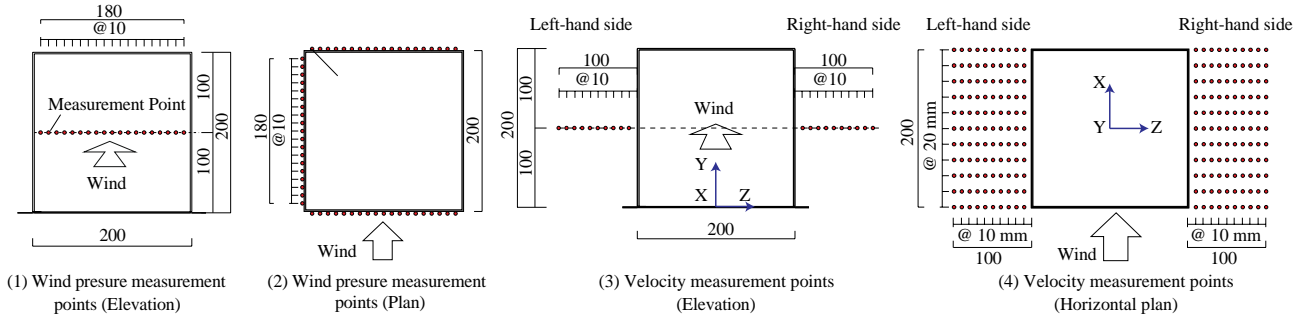
Fig. 4. Sealed model used in the wind tunnel test

(dimensions in mm, "@" indicates the interval between measurement points)

3. Comparison between measurements and CFD

3.1. Summary of numerical analysis

To investigate the fluctuating flow, CFD prediction was performed using LES. Although this study aimed to conduct a parametric study focusing on case of a small wind pressure difference, the accuracy of the numerical analysis method was first verified. The wind tunnel test presented in the previous section was analysed. The height and width of the computational domain correspond to those of the wind tunnel presented above. The length in the streamwise direction was set at 3,200 mm, that is, five times the length of the model on the windward side and ten times on the leeward side (Fig. 5). A commercial code, ANSYS Fluent 17.0, was used for the analysis. In addition to the model with openings (referred to as "opening model"), a sealed model case was also analysed to investigate wind pressure coefficients. Three cases studied in the wind tunnel experiment were simulated as opening models. Although LES was applied for all calculations, the initial flow field was obtained by applying steady-state calculation using the standard k–ε (SKE) model. This RANS calculation was run with the SIMPLE algorithm by applying the QUICK discretisation scheme for advective term. After a sufficient convergence with a residual criteria of 10^{-5}, the turbulence model was switched to LES, and the pre-conditioning unsteady calculation was performed based on the initial flow field obtained using the SKE model. The Smagorinsky-Lilly model was used, with a Smagorinsky coefficient (C_s) of 1.0. The SIMPLE algorithm was also applied for the LES calculations, but the central differencing was used for the advective differential scheme. The LES calculation was performed at time intervals of 0.0005 s for the opening model. However, in the analysis of the sealed model, time intervals of 0.0001 s were applied using a finer grid layout. The reason for this difference was that the accuracy of the wind pressure distribution was found to be improved when using a finer time interval and grid in the preliminary study, which was the main purpose of the sealed model case, although the velocity distribution remained largely constant even at time intervals of 0.0005 s. For both the sealed and opening model cases, the results of the first 1.0 s were discarded as a pre-conditioning period, and the following 10 s were adopted as the main period to calculate the flow rate and average/fluctuating component of wind pressure and velocity. Table 1 summarises the numerical settings applied in the calculations. The vertical profile of the average velocity and turbulence statistics obtained from the experiment was used together with the random flow generation technique, the spectral synthesiser, [70] to generate instantaneous velocity at the inlet boundary. Zero gauge-pressure was adopted as the outlet boundary condition.

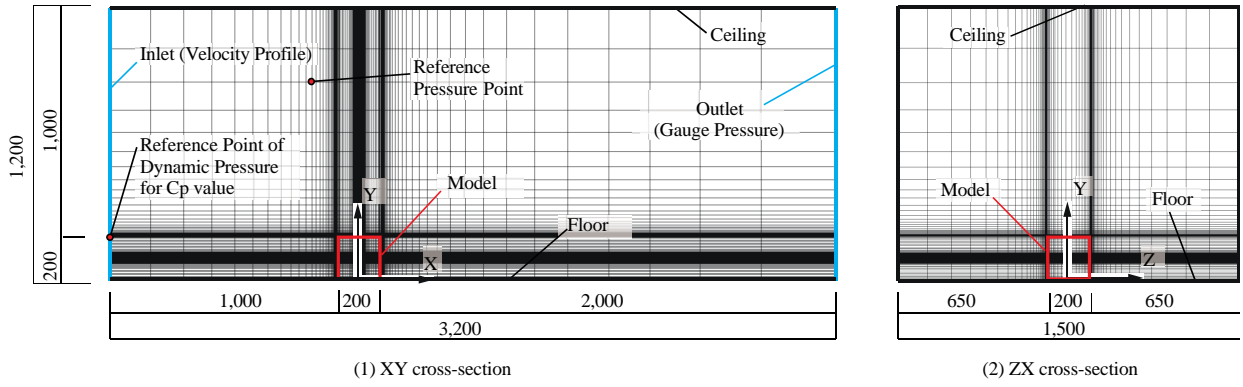(1) XY cross-section   (2) ZX cross-section

Fig. 5. Computational domain used in Large Eddy Simulation (dimensions in mm)

Table 1. Summary of method used in numerical analysis for accuracy verification

Turbulence Model		Large Eddy Simulation Smagorinsky-Lilly Model (Cs=1.0)	
CFD Code		Ansys Fluent 17.0	
Algorithm		Implicit method (SIMPLE)	
Discretization Scheme for Advection Term		Central Differencing	
Boundary Condition	Inlet	Based wind tunnel measurement and Smirnov's method	
	Outlet	Gauge Pressure : 0 [Pa]	
	Walls	Two Layer Model of Linear-Log Law	
Model		Sealed Model	Opening Model
Time Step		0.0001 [s]	0.0005 [s]
Preconditioning Calculation Term		10,000 time step (=1.0 [s])	2,000 time step (=1.0 [s])
Main Calculation Term		100,000 time step (=10 [s])	20,000 time step (=10 [s])
Total Number of Cells		1,966,720	1,753,350 (Case 1) 1,192,100 (Case 2) 1,753,350 (Case 3)

In analysing the opening case, the internal tracer concentration needs to be analysed to compare the flow rate between the CFD and wind tunnel measurements. In the present study, the particle tracing method was used, and the PFR was calculated based on the number concentration of particles. The particle tracing technique was applied instead of gas analysis because it will enable not only the calculation of the PFR, but also the obtaining of further detailed information regarding air motion and ventilation efficiency by determining the trajectories of individual particles in future studies, for example those calculating the statistics of residence time and indoor travel distance of the fresh air, probability of a contaminant returning to a room after outflow, etc. Nevertheless, the result of the particle analysis was used only to calculate the PFR as an alternative to the tracer gas in this study.

The particles used to simulate the tracer were emitted from four emission points whose positions were the same as the dosing points in the tracer gas measurement. One particle was emitted from each emission point at each time interval of the calculation, which corresponds to an emission rate of 8,000 [s^{-1}]. The Lagrangian discrete phase model was adopted to analyse inert particle motion, and the position of the particles was calculated by integrating the force balance, where only the drag force was considered, and no additional forces, such as gravity, were considered. The position of the particles was expressed as follows:

$$m_p \frac{d\overrightarrow{u_p}}{dt} = m_p F_D(\vec{u} - \overrightarrow{u_p}) \qquad (4)$$

where, m_p is the particle mass, $\vec{u}$ is the fluid-phase velocity, and $\overrightarrow{u_p}$ is the particle velocity. F_D is the drag force per unit particle mass and was calculated based on the particle density ρ_p, particle diameter d_p, relative Reynolds number Re_r, and drag coefficient C_{drag} by applying the following equation:

$$F_D = \frac{18\mu}{\rho_p d_p^2} \frac{C_{drag} Re_r}{24} \qquad (5)$$

The drag coefficient was obtained by assuming a spherical drag law[71], and Re_r is defined as

$$Re_r = \frac{d_p|\vec{u}-\overline{u_p}|}{v} \qquad (6)$$

where v is the dynamic viscosity of the air. As a physical property, the diameter of the particle was set to 1.0 μm, and the particle density was assumed to be 1.225 kg/m^3, which was the same as the air density setting with the intension to capture air movement.

For the sealed model, the horizontal distributions of the mean wind pressure coefficient, $\overline{C_p}$, on the front, lateral, and back walls were compared to those from the wind tunnel test. In addition, the mean velocity profiles around the sealed model were also compared between CFD and obtained measurement, and the measurement/monitoring points are shown in Fig. 4.

3.2. Results of accuracy verification

Because the parametric study involved investigating the wind pressure and flow rate, a comparison between the obtained measurement and CFD was performed for both the sealed and opening models in this section. In Fig. 6, the distributions of the mean wind pressure coefficient on each wall are compared. On the windward and leeward walls, a good agreement was observed. For the lateral side wall, the strong negative pressure due to the flow separation at the windward corner was slightly underestimated. However, the tendency of the wind pressure distribution could be simulated relatively well. In this sealed model, the velocity profile was compared at the side region of the model. Fig. 7 shows the results for both sides. Because an I-type hotwire probe was used in the measurement, and it was set with the wire parallel to the Z axis, the experimental results seemed to record the velocity resulting from the X and Y components. For a rational comparison, the corresponding 2-D velocity resultant, $\overline{v_{xy}}$, was calculated from the LES results based on the following equation:

$$\overline{v_{xy}} = \overline{\sqrt{v_x^2 + v_y^2}} \qquad (7)$$

where, v_x and v_y are the X and Y components of the instantaneous grid scale velocity of the LES, respectively, and the overbar indicates the time-average. The CFD results for the velocity profile are consistent with the experimental results, although a slight overestimation was observed. Thus, the accuracy of the LES for the sealed model was verified.
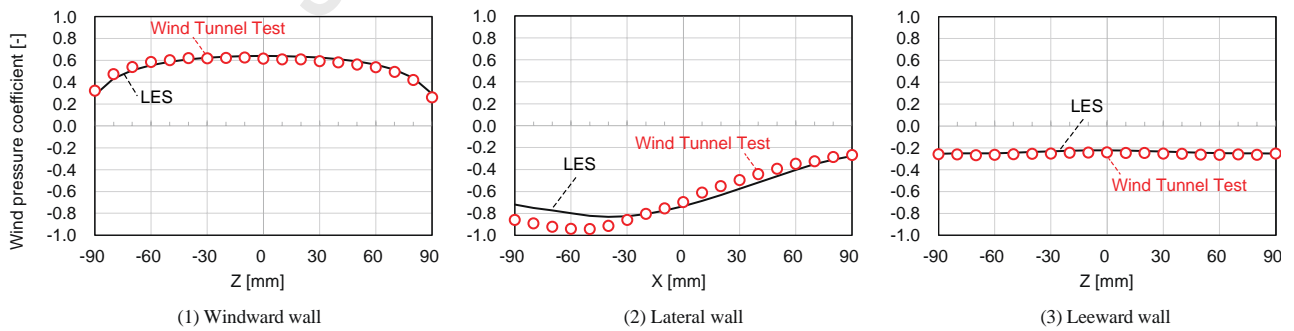

Fig. 6. Comparison of mean wind pressure coefficient between CFD and obtained measurement
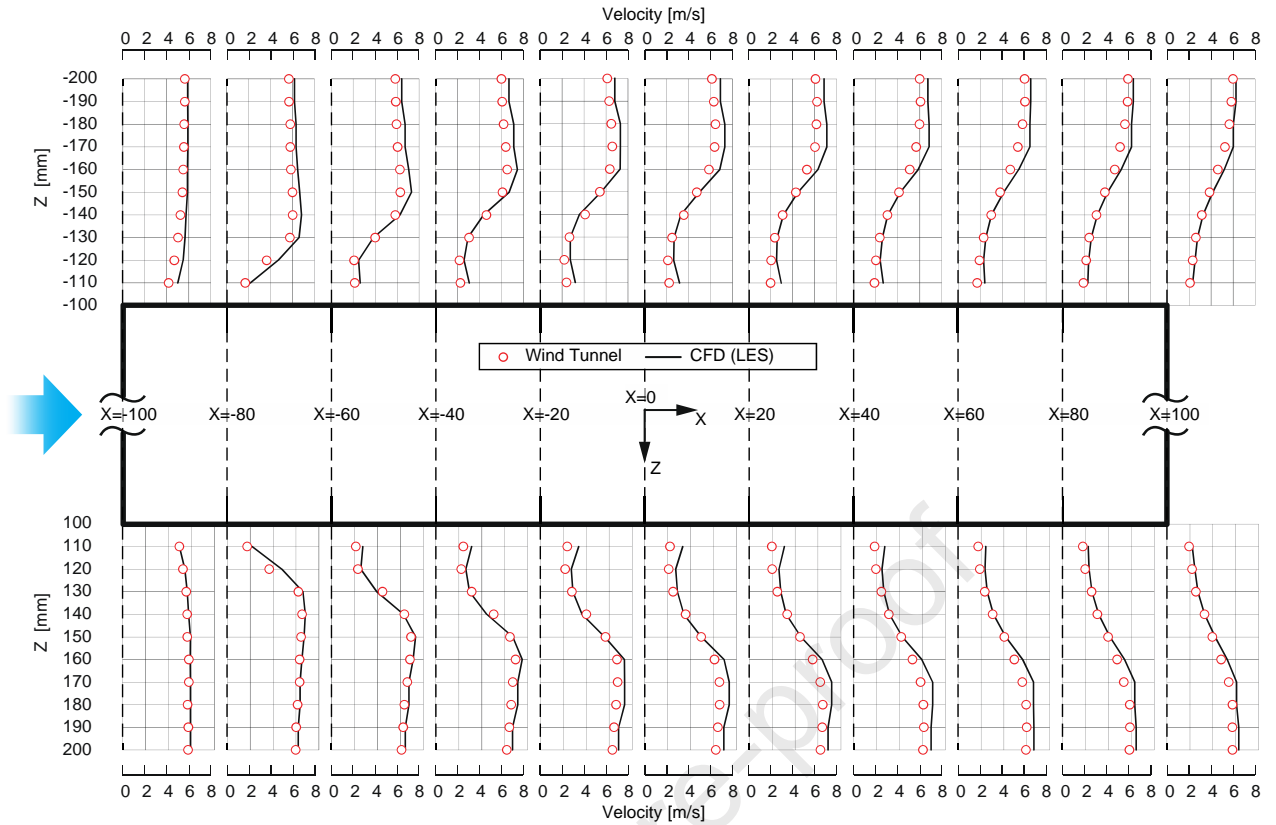
Fig. 7. Profiles of 2-D velocity resultant, $\overline{v_{xy}}$, at the side of the
model obtained from hotwire measurement and LES

Fig.8 (1) shows extracted examples of the particle distribution and instantaneous velocity distribution, which are the results of Case 2 at a flow time of 1.0 to 5.0 s. The instantaneous velocity distribution shows the flow direction from Opening 1 to Opening 2 at a flow time of t=1.0 s and the opposite direction at t=2.0 s. This was regarded as the pulsating flow which occurs in the case of two openings [44,47] and can be interpreted as an instantaneous cross-ventilation phenomenon with alternating flow directions. As this is a fluctuation and is driven by the instantaneous wind pressure difference, the standard deviation of the wind pressure coefficient ($\sigma_{\Delta Cp}$) was a key parameter. On the other hand, at t=5.0 s, an external airflow parallel to the lateral wall was observed around both openings, and the inflow and outflow were not clear at Opening 1 and 2. This is regarded as the flow field assumed by Warren [49], and the mechanism of ventilation is explained by turbulent mixing by eddy penetration, where the external velocity around the opening is a key parameter.

Regarding the particles analysis, because the instantaneous coordinates were all known, the particles existing inside the room model were counted every 1 s to calculate the average particle-number concentration within the room and the PFR based on the LES. However, it must be noted that this was not a strict comparison with the experimental results, but rather a relative comparison, that is, in the measurement, even though 12 sampling holes were created at three different heights to measure the average concentration, only one sampling tube was installed at the centre of the model. As a qualitative tendency, the particles spread over the entire area inside the model after a flow time of 4.0 s. Because the number of particles inside the room continued to increase during the main calculation term of 10 s, the steady-state particle concentration could not be obtained from this main calculation time. To enable comparison of the PFR with the experimental results, the following equation based on the assumption of perfect mixing was applied, and the air change rate, n, was estimated using the least-squares method.

$$C_r(t) = \frac{m}{nV_r}(1 - e^{-nt}) \qquad (8)$$

where, C_r (t) is the number concentration [m^{-3}], V_r is the room volume [m^3], and t is the elapsed time [s] of the main calculation.

Fig. 8 (2) shows the response of the particle-number concentration for each case of the opening models. Here, the fitting curve for each case based on Eq. (8) was also added. The PFR was calculated based on the air change rate estimated using LES and the room air volume. Fig. 8 (3) shows the response of the tracer-gas concentration recorded in the wind tunnel test, and the PFR was also obtained from the mean value of CO_2 concentration after emission, as explained in Section 2.2. Fig. 8 (4) compares the PFR between the obtained measurement and LES for each of the three cases. In general, the PFR obtained from CFD was smaller than that obtained from the measurement. As mentioned above, the wind tunnel experiment evaluated the concentration at the central position of the room model, and the measured PFR could not be strictly compared with that of CFD which evaluates the spatial average concentration. Considering that the location of opening 1 was fixed at the centre of the lateral wall, the central position inside the model where the sampling tube existed in the measurement may have a somewhat lower concentration, leading to an overestimation of the PFR. As a general tendency of the experimental results, Case 2 resulted in a slightly larger but almost the same PFR when compared with Case 1, whereas Case 3 showed a larger flow rate than did the other two cases. According to the experimental results in Fig. 6 (2), the mean wind pressure coefficient differences ($\Delta\overline{C_p}$) in Cases 1, 2, and 3 were 0.244, 0, and 0.348, respectively, assuming the symmetry, which led to the largest PFR in Case 3. This indicates that the ventilation was more or less driven by the mean wind pressure difference in Case 3. Considering the result of $\Delta\overline{C_p}$, it should be noted that Case 2 showed almost the same flow rate as did Case 1 despite no mean wind pressure difference being present. As discussed in the previous paragraph, pulsating flow and turbulent mixing were the main factors which caused ventilation in Case 2. The same tendency was observed in the LES results. Although the verification was limited to a relative comparison regarding the PFR, because the tendency was generally reproduced, further cases were investigated as a parametric study varying the position of openings and focusing on the conditions of a small wind pressure difference in the following section, applying the numerical setting method adopted in this study.
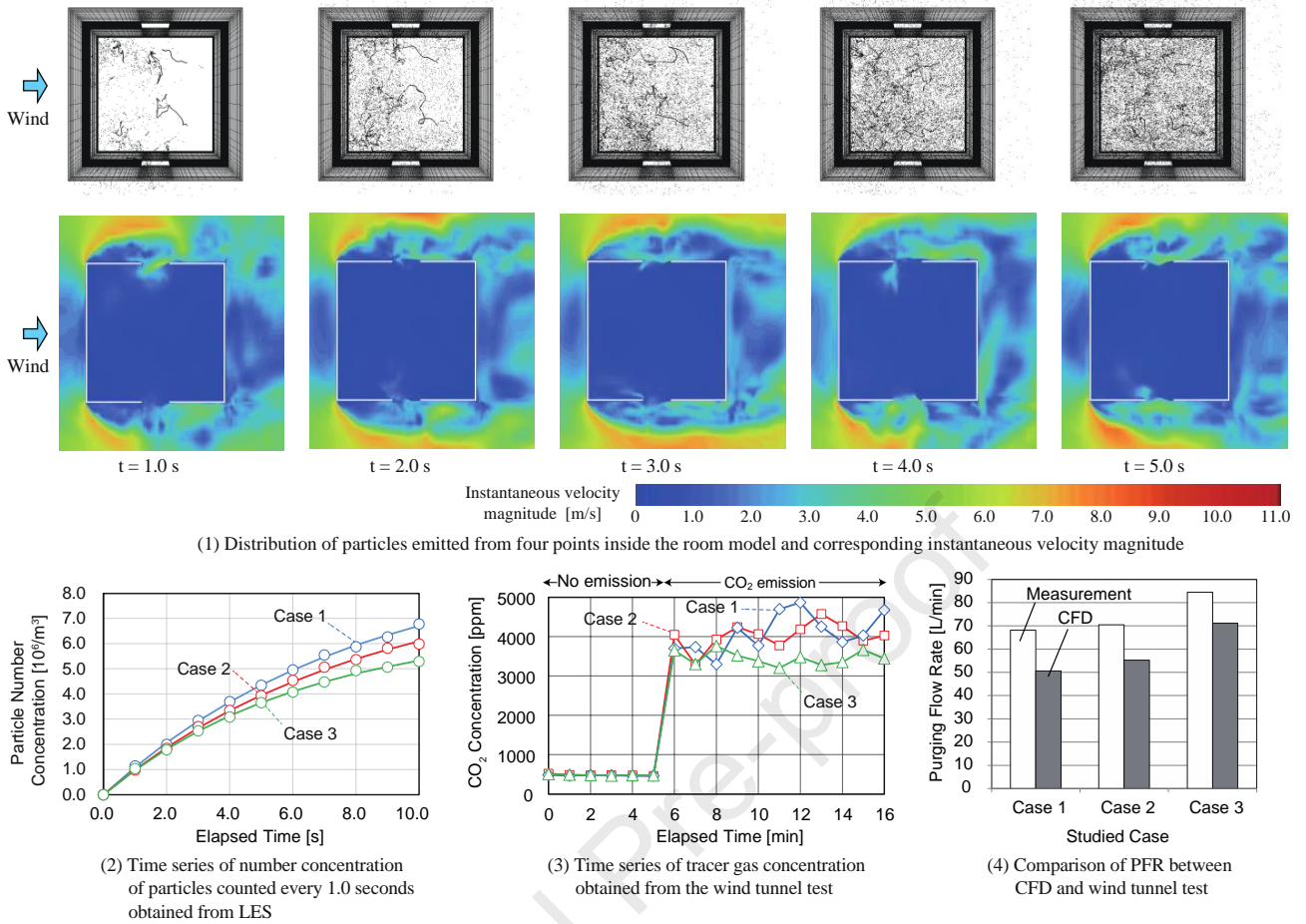
(1) Distribution of particles emitted from four points inside the room model and corresponding instantaneous velocity magnitude

(2) Time series of number concentration of particles counted every 1.0 seconds obtained from LES

(3) Time series of tracer gas concentration obtained from the wind tunnel test

(4) Comparison of PFR between CFD and wind tunnel test

Fig. 8. Comparison of tracer gas concentration and purging flow rate (PFR) between wind tunnel experiment and CFD

4. Parametric study with varying opening positions

4.1. Outline of the analysis

As mentioned above, a parametric study was conducted using LES to analyse the flow rate under small wind pressure differences. In all cases, a cubic model equipped with two openings was analysed, and the position of the openings was varied. The basic configuration of the model was the same as that described in the previous section, and each opening had a side length of 40 mm. The studied cases were classified into four types according to the opening arrangement (Fig. 9), where both the double- and single-sided cases were analysed. In total, 19 cases were simulated by varying the positions of the openings so that the wind pressure difference between openings decreased. Ten cases of double-sided openings were studied (Case DS), five of which had symmetrical opening arrangements (Cases DS 0-0 to DS 0-4), and the rest had asymmetric opening arrangements (Cases DS 1 to DS 5). Regarding the single-sided openings, the studied cases were divided into three types: two openings on the front wall (Case SS-F), a lateral side wall (Case SS-L), and a back wall (Case SS-B). Table 2 provides detailed information of all cases and shows the result of the flow rate for both the PFR and AFR, the ratio of which is also presented. In addition, from the LES result for the sealed model presented in the previous section, the mean wind pressure coefficient difference between the two openings $\Delta\overline{C_p}$, standard deviation of the wind pressure coefficient $\sigma_{\Delta Cp}$, and velocity in the vicinity of the assumed opening position obtained 20.0 mm from the model wall V_{vic}, are summarised in the table. The size of the computational domain was the same as that illustrated in Fig. 5, and

the same boundary conditions were applied. The LES method was the same as that described in the previous section, where the calculated flow time duration was 1.0 s for the pre-conditioning term and 10.0 s for the main calculation, and the time step size was 0.0005 s.

In the present study, the flow rate was mainly evaluated using the AFR, which is based on instantaneous velocity, because one of the primary objectives of this work was on the applicability of the Orifice equation, which cannot include the effect of ventilation efficiency defined by contaminant concentration or age of air, but only considers the bulk airflow. To calculate the AFR, the instantaneous velocity component perpendicular to the opening was monitored at 64 (8×8) points at each of the two openings in all the cases (Fig. 10). This enabled the calculation of the instantaneous rates of both the inflow and outflow at each time interval, which were expressed as Q_{in} and Q_{out}, respectively. Namely, Q_{in} was obtained by integrating the instantaneous velocity over the opening only if the flow direction showed an inflow. Q_{out} was obtained in the same way, that is, by integrating the instantaneous outflow velocity. Although the position of the monitoring points for instantaneous velocity did not strictly correspond to the computational grid layout at the opening, Q_{in} and Q_{out} were approximately balanced. The absolute values of these two flow rates were averaged to define the instantaneous airflow rate. Then, AFR in the present study was then obtained by taking the time average as follows:

$$AFR = \frac{\overline{(|Q_{in}|+|Q_{out}|)}}{2} \qquad (9)$$

While the AFR needs to be used to evaluate the discrepancy in the bulk airflow rate predicted by the Orifice equation, the difference between the effective ventilation rate and the bulk airflow rate is also of great importance, which will be discussed in terms of ventilation efficiency. Therefore, the PFR, used as the effective ventilation rate, was also calculated in each case as additional information, and the particle tracking method was adopted, as described in the previous section. Here, particles were generated at each time interval at 27 points within the model (Fig. 10), with the intention of creating a uniform emission to analyse the PFR, indicating that 540,000 particles were generated and tracked throughout the main calculation for 10 s. Here, calculating the PFR with uniform generation can also be interpreted essentially as evaluating the spatially averaged age of air within the room with a dimension of flow rates.
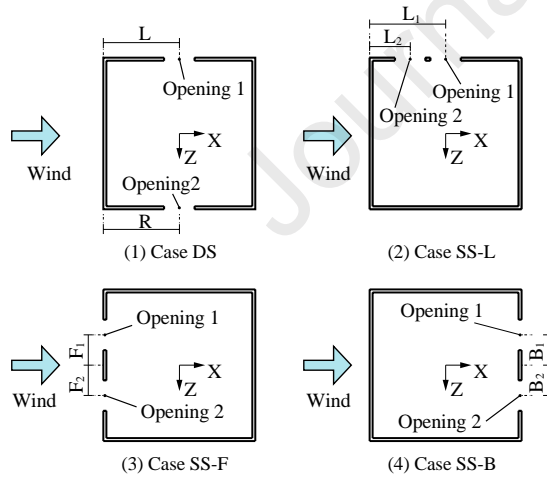

Fig. 9. Classification of studied cases in the parametric study using LES

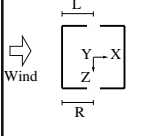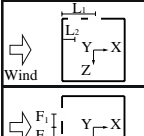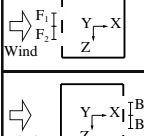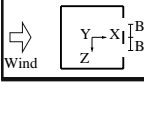| Particle Generation Point			
X Coordinate [mm]	-66	0	66
Y Coordinate [mm]	33	100	166
Z Coordinate [mm]	-66	0	66
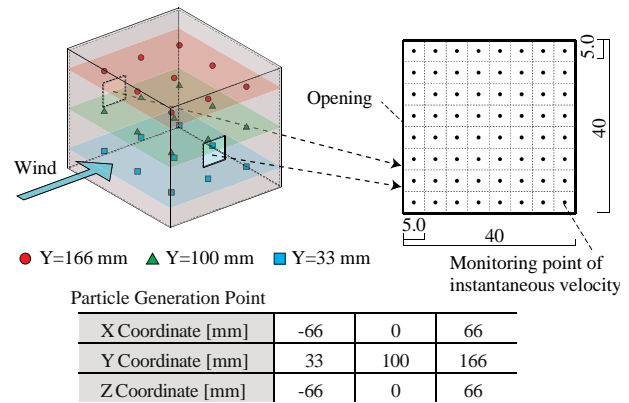
Figure 10. Particle generation points inside the room and monitoring points of instantaneous velocity at the opening (dimensions in mm)

Table 2 Detailed information of the studied cases and results of the AFR and PFR obtained using LES

Description	Case ID	Central Position of Opening (X, Y, Z) [mm]		Cp and mean velocity in its vicinity				$\overline{\Delta Cp}$ [-]	$\sigma_{\Delta Cp}$ [-]	AFR [L/min]	PFR [L/min]	PFR/AFR [%]
				Opening 1		Opening 2						
		Opening 1	Opening 2	$\overline{Cp}$ [-]	Vvic [m/s]	$\overline{Cp}$ [-]	Vvic [m/s]					
	DS 0-0	L=100 (0, 100, -100)	R=100 (0, 100, 100)	-0.73	1.41	-0.74	1.39	0.007	0.236	112.1	88.1	78.59
	DS 0-1	L=80 (-20, 100, -100)	R=80 (-20, 100, 100)	-0.81	1.47	-0.82	1.48	0.012	0.221	99.8	74.8	75.03
	DS 0-2	L=60 (-40, 100, -100)	R=60 (-40, 100, 100)	-0.83	1.31	-0.84	1.33	0.007	0.201	88.9	62.1	69.78
	DS 0-3	L=120 (20, 100, -100)	R=120 (20, 100, 100)	-0.63	1.23	-0.63	1.15	0.001	0.244	123.0	96.8	78.67
	DS 0-4	L=140 (40, 100, -100)	R=140 (40, 100, 100)	-0.52	0.85	-0.51	0.81	0.010	0.247	135.0	106.8	79.08
	DS 1	L=80 (-20, 100, -100)	R=100 (0, 100, 100)	-0.81	1.47	-0.74	1.39	0.065	0.229	111.7	78.0	69.84
	DS 2	L=80 (-20, 100, -100)	R=40 (-60, 100, 100)	-0.81	1.47	-0.81	1.11	0.003	0.206	95.4	67.5	70.83
	DS 3	L=80 (-20, 100, -100)	R=120 (20, 100, 100)	-0.81	1.47	-0.63	1.15	0.173	0.237	124.6	89.5	71.77
	DS 4	L=80 (-20, 100, -100)	R=130 (30, 100, 100)	-0.81	1.47	-0.57	0.99	0.236	0.237	134.6	98.1	72.89
	DS 5	L=80 (-20, 100, -100)	R=140 (40, 100, 100)	-0.81	1.47	-0.51	0.81	0.299	0.234	149.6	115.9	77.49
	SS-L1	L_1=100 (0, 100, -100)	L_2=50 (-50, 100, -100)	-0.73	1.41	-0.82	1.18	0.089	0.235	95.8	58.0	60.51
	SS-L2	L_1=100 (0, 100, -100)	L_2=40 (-60, 100, -100)	-0.73	1.41	-0.80	1.16	0.065	0.218	98.9	61.2	61.82
	SS-L3	L_1=100 (0, 100, -100)	L_2=30 (-70, 100, -100)	-0.73	1.41	-0.77	1.37	0.040	0.199	100.5	62.1	61.77
	SS-F1	F_1=30 (-100, 100, -30)	F_2=30 (-100, 100, 30)	0.62	2.13	0.62	2.13	0.001	0.048	80.9	76.2	94.16
	SS-F2	F_1=40 (-100 ,100, -40)	F_2=40 (-100, 100, 40)	0.61	2.29	0.61	2.28	0.002	0.061	86.2	80.8	93.66
	SS-F3	F_1=50 (-100, 100, -50)	F_2=50 (-100, 100, 50)	0.59	2.49	0.59	2.47	0.003	0.071	90.3	80.3	88.97
	SS-B1	B_1=(100, 100, -30)	B_2=30 (100, 100, 30)	-0.23	1.17	-0.23	1.25	0.002	0.057	56.4	52.0	92.20
	SS-B2	B_1=(100, 100, -40)	B_2=40 (100, 100, 40)	-0.24	1.26	-0.24	1.34	0.001	0.068	60.0	55.7	92.83
	SS-B3	B_1=(100, 100, -50)	B_2=50 (100, 100, 50)	-0.24	1.33	-0.24	1.37	0.000	0.078	64.8	55.7	85.92

4.2. Results and Discussion

Fig. 11 (1) shows the fluctuation of the instantaneous flow rate, Q_{in} and Q_{out}, and their sum during the first 2.0 s of the main calculation in Case DS 0-0, where the inflow was expressed as a positive value. Although mass balance was not strictly maintained because of the difference between the monitoring points and computational grids over the openings, the difference between the inflow and outflow was not significant and was almost negligible. Thus, the arrangement of 64 instantaneous velocity monitoring points at each opening was considered acceptable for calculating the AFR.

In Fig. 11 (2), the correlations between the mean wind pressure coefficient difference, $\Delta\overline{C_p}$, and two types of flow rates, the PFR and AFR, are shown for five cases, DS 1 to DS 5. The flow rate estimated using the conventional Orifice equation based on Eq.(1) was also added, where the discharge coefficient of the opening, C_d, was assumed to be 0.65 for each opening, which indicates a $(C_d A_W)_{connected}$ of 0.000735 m^2 in Eq.(1). Comparing the PFR with AFR, the PFR was estimated to be approximately 70–80% of the AFR in the five cases of double-sided openings. This difference indicates the ventilation effectiveness, meaning that not all parts of the AFR can contribute to purging contaminants. According to the PFR divided by the AFR shown in Table 2, the rest of the Case DS also resulted in the same range of ventilation effectiveness. For the single-sided conditions, however, Case SS-L resulted in a ventilation effectiveness of approximately 60 %, which is lower than the Case DS series, while Cases SS-F and SS-B each showed an effectiveness of approximately 85-95 %. These differences in the PFR/AFR are more or less related to the flow patterns inside and outside the room. Fig. 12 shows the instantaneous velocity vector plots with the static pressure distribution at flow times of t=1.0, 3.0, and 5.0 in the main calculation. Here, the reference pressure point was taken at X, Y, Z = -200, 800, and 0 mm, respectively. In cases of double-sided openings, the inflow and outflow occur alternately at each opening, and the airflow travels inside the room. However, because the airflow does not spread throughout the entire room, the PFR cannot exceed the AFR, and their ratio ranged from 0.7–0.8 in the cases studied here. Focusing on the single-sided openings on the lateral wall, the flow direction diagonal to the opening was observed. Since two openings are located close to each other, part of inflow directly flows toward the other opening before spreading through the room, which can be expressed as the "flow contact" [25], which causes short-circuiting between openings in this case. This appeared to have caused decrease in the PFR/AFR in the SS-L series, resulting in an effectiveness of approximately 60 %. However, in Cases SS-F and SS-B, as a qualitative tendency, no inflow directly toward the other opening was observed, and the inflow travelled through the room. Because the other opening exists on the same façade of the inflow opening, the air flowing into the room more easily spreads through the whole room, leading to a relatively higher PFR/AFR of approximately 85–95%. Thus, the ventilation efficiency of the two openings for the single-sided ventilation differed depending on the location of the openings in the external wind direction.

Given the definitions of the PFR and AFR, particles short-circuiting caused a decrease in ventilation efficiency, as mentioned above. For further quantitative investigation in the future studies, analysing the length of trajectories from the opening will be useful. Another possible factor causing the difference between the AFR and PFR is that the contaminant returns to the room after it flows out of the opening. This must be somewhat affected by the external flow pattern around the opening. In other words, if the contaminant immediately flows downstream, fewer contaminants return to the room, but if the air tends to stagnate in front of the opening, the inflow includes more contaminants, leading to low ventilation effectiveness. Albuquerque et al. [64] performed LES for simulations of single-sided ventilation with two openings where window separation was varied, and reported that the ventilation effectiveness (effective ventilation rate divided by bulk airflow rate) ranged from 60% to 75%, which is lower than that of Case SS-B in the present study. An additional factor that may lead to differences in ventilation effectiveness is the shape of the opening. Because only simple square openings were considered in this study, the type of windows should also be considered as a parameter which may affect the external airflow pattern and the difference between the AFR and PFR.

According to the results of the five cases presented in Fig. 11 (2), the Orifice equation cannot accurately predict the AFR when the mean wind pressure coefficient difference is low. The flow rate estimated using the Orifice equation was approximately 16.3% and 64.8% of the AFR calculated using LES in Cases DS 2 ($\Delta\overline{C_p}$=0.003) and DS 1 ($\Delta\overline{C_p}$=0.065),

respectively. In Case DS 3, where $\Delta\overline{C_p}$=0.173, this percentage was 94.7%, and shows much less underestimation. Because the main driving force of wind-induced ventilation is turbulence when the mean pressure difference is low, using the Orifice equation is not appropriate for these two cases. Fig. 11 (3) shows the AFR obtained for all cases studied here. This results also showed that the AFR does not follow the Orifice equation when $\Delta\overline{C_p}$ is low, and that there are other parameters regarding turbulence that can explain the difference in flow rates. As discussed in Section 3.2, we assumed that it was necessary to consider two phenomena, namely pulsating flow and turbulent mixing by eddy penetration, in wind-induced natural ventilation with a small mean wind pressure difference. Consequently, as a parameter of importance, the standard deviation of the instantaneous difference in the wind pressure coefficient (expressed as $\sigma_{\Delta Cp}$), was considered first because it can cause a pulsating flow between the two openings[44]. Fig. 11 (4) shows the results for $\sigma_{\Delta Cp}$ and the corresponding AFR. In general, the AFR increases when $\sigma_{\Delta Cp}$ was large. Assuming a low difference in the mean wind pressure between openings, a large $\sigma_{\Delta Cp}$ leads to the instantaneous cross-ventilation in the alternating direction. Thus, $\sigma_{\Delta Cp}$ considerably affects the AFR. Nevertheless, it should also be noted that different AFR results can be observed even when $\Delta\overline{C_p}$ and $\sigma_{\Delta Cp}$ are almost the same. Focusing on the three cases for Cases SS-F and SS-B, Case SS-F always showed a larger AFR than did Case SS-B, even when their $\sigma_{\Delta Cp}$ values were similar. In these cases, $\Delta\overline{C_p}$ was almost zero because the arrangements of the openings were symmetric. Consequently, to predict the flow rate, it is rational to consider an additional parameter which explains the ventilation mechanism caused by turbulence.

(1) Instantaneous value of inflow and
outflow rate in Case DS 0-0

(2) Comparison of AFR and PFR in Case DS 1 to 5
with the flow rate estimated from orifice equation

(3) Correlation between mean AFR and mean wind
pressure coefficient difference in all cases studied

(4) AFR and standard deviation of instantaneous
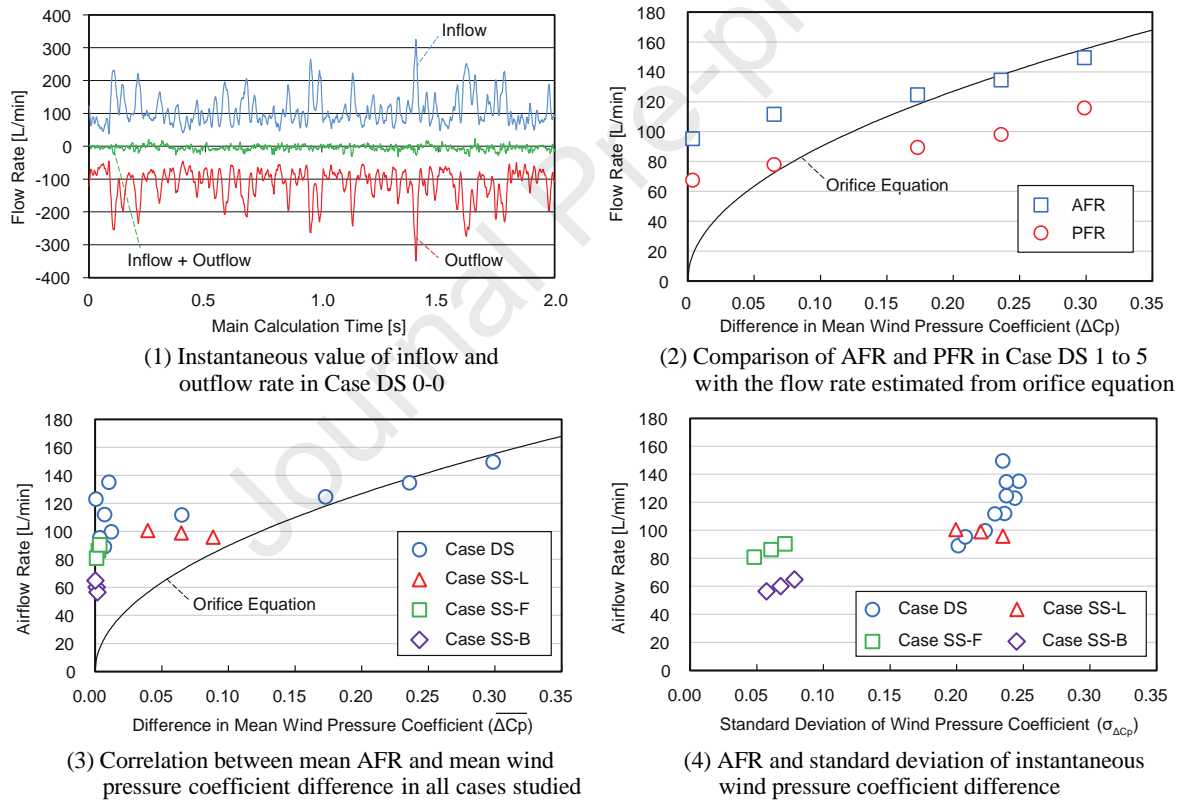wind pressure coefficient difference

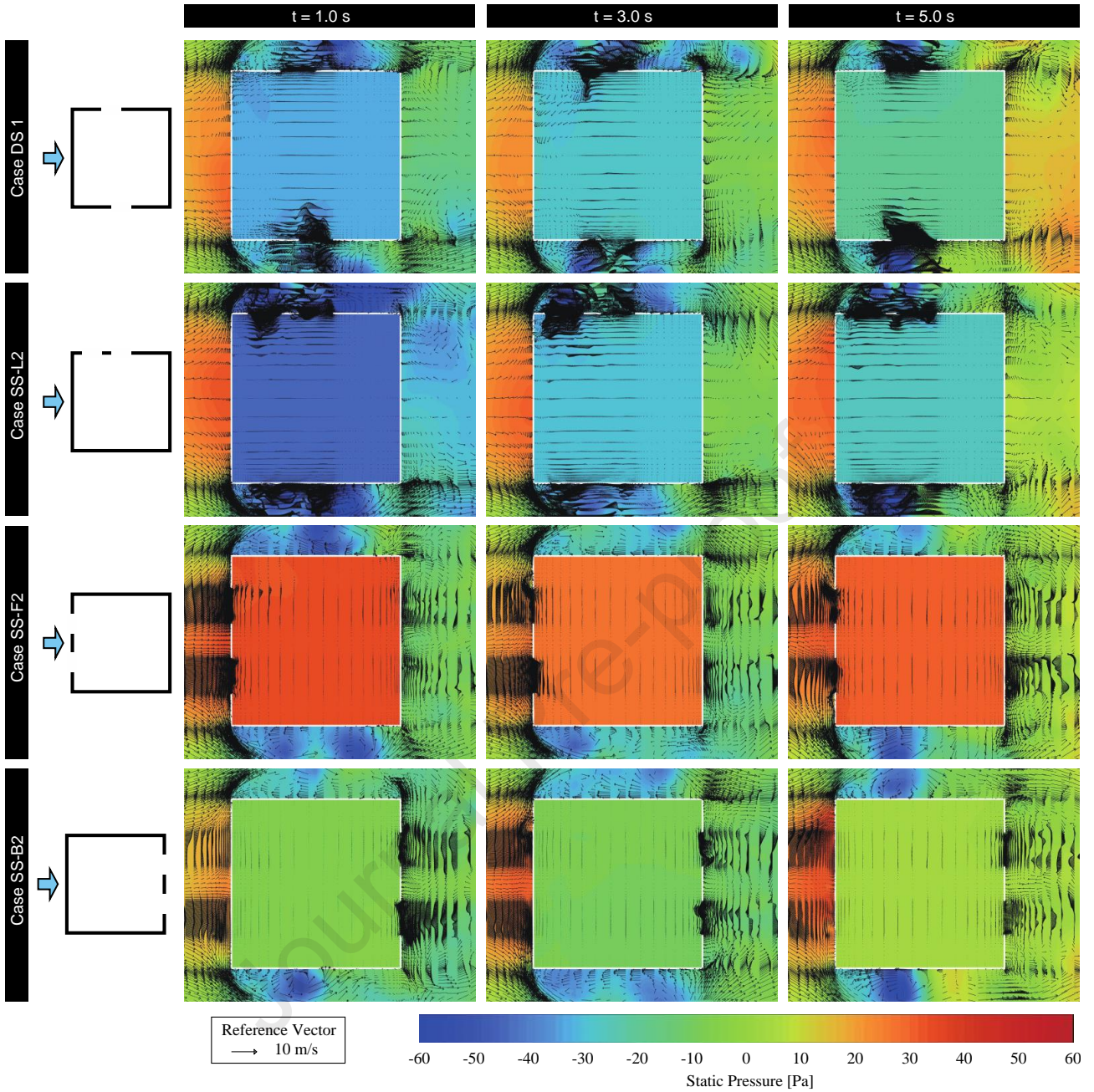Fig.11. Results related with flow rate obtained using LES

Fig.12. Instantaneous velocity vector with static pressure distribution for double-sided openings and single sided openings on lateral, front and back walls

By including the standard deviation of the wind pressure coefficient difference as a parameter into the Orifice equation, Daish et al. [42] proposed the following formula:

$$Q = A_{ref} V_{ref} \sqrt{a_p \left| \overline{\Delta C_p} \right| + a_\sigma \sigma_{\Delta Cp}} \qquad (10)$$

where, A_{ref} is the characteristic opening area, and a_p and a_σ are the correlation constants. Although this equation can reflect the effect of the fluctuating wind pressure difference between openings, it cannot explain the difference between Cases SS-F and SS-B. Given the factors of air exchange[45], eddy penetration can be another important parameter to be considered, which has often been treated using the mixing layer theory mainly for the cases of the single opening. The

basic approach of the mixing layer theory assumes that the flow rate is proportional to the opening area and external free-stream velocity. In this study, to obtain a simplified modification of Eq.(1) and also Eq.(10), the following equation is proposed:

$$Q = (C_d A_W)_{connected} V_{ref} \sqrt{a_p \left| \overline{\Delta C_p} \right| + a_\sigma \sigma_{\Delta Cp}} + \Sigma a_e A_W V_{vic} \qquad (11)$$

where, a_e denotes an additional model constant. V_{vic} is the external local velocity near the assumed opening position which was obtained from the sealed model. As mentioned above, the position adopted to acquire V_{vic} was 20 mm from the wall at the centre of the assumed opening position, which was half of the side length of the opening. Here, the velocity magnitude obtained from three mean velocity components was taken as V_{vic}. The combination of constants, a_p, a_σ, and a_e to achieve the best agreement with the LES results for the studied 19 cases was determined using the least-squares method, and we obtained a_p=0.285, a_σ=0.402, and a_e=0.0768.

Fig. 13 compares the AFR between the LES and simplified estimation using Eq.(11), where the range of the ±30% error is indicated by dashed lines. Adding the last term to Eq.(11) to explain the effect of eddy penetration resulted in different AFRs between Case SS-B and Case SS-F for the case of similar $\sigma_{\Delta Cp}$ values. For Case SS-L, the AFR predicted using Eq.(11) showed somewhat larger variance than did LES but still showed relatively good agreement within ±30% error, which is the same criterion by Daish et al.[42]. For Case DS, the three cases with the largest flow rates predicted by Eq.(11) corresponded to the three cases with the largest $\Delta \overline{C_p}$ (Cases DS 5, DS 4, and DS 3).
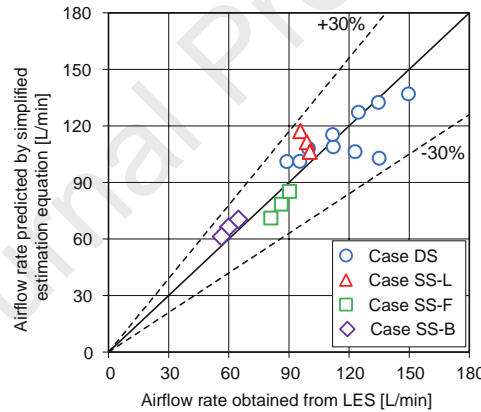

Fig. 13. Comparison of the AFR obtained
using LES and Eq.(11)

It must be noted that this modified equation is not for predicting PFR but for AFR because it is the bulk airflow rate obtained based on ventilation mechanics using pressure difference, that is, the effect of ventilation efficiency cannot be considered. According to its definition, the flow rate contributing to ventilation is PFR. Therefore, to evaluate natural ventilation performance for cases with a small wind pressure difference, there must be two steps, that is, 1) estimating AFR considering the effect of turbulence, then 2) evaluating the ventilation efficiency (PFR/AFR). To address the former, Eq.(11) was proposed, and the approach of modifying the Orifice equation considering both pulsating flow and eddy penetration can work relatively well for the studied cases with small wind pressure differences. However, since the maximum value of $\Delta \overline{C_p}$ studied in the present study was 0.299, there still remains a question regarding the extent to which the higher $\Delta \overline{C_p}$ proposed equation is valid. In addition, the $\sigma_{\Delta Cp}$ studied here ranged between 0.048 and 0.247, which may not be sufficiently large to confirm their general applicability. This means that there is a limitation of the proposed equation for the simple room case within these ranges of $\Delta \overline{C_p}$ and $\sigma_{\Delta Cp}$. Therefore, further studies should

determine the appropriate condition for switching the equation to the standard Orifice equation. For studies to investigate this, for example, the analyses of the sheltered condition of surrounding buildings and other shapes of the target building may be effective because they provide wider range $\Delta\overline{C_p}$ and $\sigma_{\Delta Cp}$. For the latter step, evaluating the ventilation efficiency (PFR/AFR), the difference in tendency caused by opening arrangement was clearly shown in this study, which has not been sufficiently investigated in the research field. Evaluating this ratio could lead to a new index of ventilation efficiency for natural ventilation phenomena. In this context, the results obtained in this study provide important information. However, to enable estimation of this ratio in more practical situations, more systematic investigations are necessary for acquiring further understanding of its mechanism. As discussed above, analysing trajectories in the future studies is helpful because it is important to separately consider the airflow pattern travelling from the inlet and the contaminant returning to the room after outflow, which is difficult only by analysing the gaseous scalar field.

5. Summary and future prospects

Wind-induced natural ventilation rate is generally estimated using the standard Orifice equation; however, this equation is not suitable when turbulence is the dominant driving force. This study focused on the case of ventilation with two openings where the difference in the mean wind pressure coefficient between openings, $\Delta\overline{C_p}$, is small. Furthermore, this study investigated the isolated single-room building model using LES, the accuracy of which was determined by comparing results with wind tunnel experiments. The purging flow rate (PFR) and airflow rate (AFR) were evaluated as the effective ventilation and bulk airflow rates, respectively. A parametric study was performed by varying the position of the openings, which correspondingly varied $\Delta\overline{C_p}$ and other two additional parameters, namely the standard deviation of instantaneous wind pressure coefficient difference, $\sigma_{\Delta Cp}$, and external velocity in the vicinity of the opening, V_{vic}. Assuming that these two parameters can explain the characteristics of two major factors of ventilation caused by turbulence, pulsating flow, and eddy penetration, a modification of the standard Orifice equation to estimate AFR was proposed, and three model constants were obtained. The major findings of this study are summarised as follows.

- The AFR estimated using the standard Orifice equation was 64.8 % of that calculated using LES in the case where $\Delta\overline{C_p}$=0.065, whereas it was 94.7% when $\Delta\overline{C_p}$=0.173. A lower $\Delta\overline{C_p}$ led to a larger range of variance in this estimation error.
- Among the cases studied, the ventilation effectiveness (PFR/AFR) in the cases of double-sided openings (Case DS) ranged from 70–80%, whereas it differed in the single-sided cases depending on the façade where openings were provided, i.e., approximately 60% for lateral side and 90% for windward (Case SS-F) and leeward sides (Case SS-B).
- Even when $\Delta\overline{C_p}$ was almost zero and $\sigma_{\Delta Cp}$ remained almost the same, the AFR differed, and Case SS-F showed a larger AFR than did Case SS-B.
- The proposed simplified equation could estimate the AFR within an error of ±30% from that of LES, including Cases SS-F and SSB, where both $\Delta\overline{C_p}$ and $\sigma_{\Delta Cp}$ remained almost the same.

However, there are still some challenges and limitations to the findings described above. Because the effective ventilation rate is important in terms of ventilation performance, the ratio of PFR to AFR must be predicted, even if the AFR was well predicted. Therefore, further studies should acquire an understanding of the relationship between building/opening conditions and physical phenomena, such as indoor airflow short-circuiting and contaminant return after outflow. Analysing the trajectories of individual particles could be beneficial for investigating this in detail. In addition, because simple square openings were studied without changing the opening size, the effects of window type and porosity should also be studied in future studies. To improve the generality of the proposed equation for estimating the AFR, more systematic parametric studies should be performed using wider ranges of $\Delta\overline{C_p}$ and $\sigma_{\Delta Cp}$. From this perspective, for instance, the building shape and surrounding buildings could be changed as parameters.

Acknowledgement

References

[1]   M. Kolokotroni, A. Aronis, Cooling-energy reduction in air-conditioned offices by using night ventilation, Appl Energy. 63 (1999) 241–253. https://doi.org/10.1016/S0306-2619(99)00031-8.

[2]   P. Heiselberg, M. Perino, Short-term airing by natural ventilation - implication on IAQ and thermal comfort, Indoor Air. 20 (2010) 126–140. https://doi.org/10.1111/J.1600-0668.2009.00630.X.

[3]   S. D'Oca, V. Fabi, S.P. Corgnati, R.K. Andersen, Effect of thermostat and window opening occupant behavior models on energy use in homes, Building Simulation 2014 7:6. 7 (2014) 683–694. https://doi.org/10.1007/S12273-014-0191-6.

[4]   L. Wang, S. Greenberg, Window operation and impacts on building energy consumption, Energy Build. 92 (2015) 313–321. https://doi.org/10.1016/J.ENBUILD.2015.01.060.

[5]   M.J. Sorgato, A.P. Melo, R. Lamberts, The effect of window opening ventilation control on residential building energy consumption, Energy Build. 133 (2016) 1–13. https://doi.org/10.1016/J.ENBUILD.2016.09.059.

[6]   T. Psomas, M. Fiorentini, G. Kokogiannakis, P. Heiselberg, Ventilative cooling through automated window opening control systems to address thermal discomfort risk during the summer period: Framework, simulation and parametric analysis, Energy Build. 153 (2017) 18–30. https://doi.org/10.1016/J.ENBUILD.2017.07.088.

[7]   E. Gratia, A. de Herde, Natural cooling strategies efficiency in an office building with a double-skin façade, Energy Build. 36 (2004) 1139–1152. https://doi.org/10.1016/J.ENBUILD.2004.05.004.

[8]   T. Kobayashi, M. Sandberg, H. Kotani, L. Claesson, Experimental investigation and CFD analysis of cross-ventilated flow through single room detached house model, Build Environ. 45 (2010) 2723–2734. https://doi.org/10.1016/J.BUILDENV.2010.06.001.

[9]   P. Karava, T. Stathopoulos, A.K. Athienitis, Airflow assessment in cross-ventilated buildings with operable façade elements, Build Environ. 46 (2011) 266–279. https://doi.org/10.1016/J.BUILDENV.2010.07.022.

[10]   R. Ramponi, B. Blocken, CFD simulation of cross-ventilation flow for different isolated building configurations: Validation with wind tunnel measurements and analysis of physical and numerical diffusion effects, Journal of Wind Engineering and Industrial Aerodynamics. 104–106 (2012) 408–418. https://doi.org/10.1016/J.JWEIA.2012.02.005.

[11]   T. van Hooff, B. Blocken, Y. Tominaga, On the accuracy of CFD simulations of cross-ventilation flows for a generic isolated building: Comparison of RANS, LES and experiments, Build Environ. 114 (2017) 148–165. https://doi.org/10.1016/J.BUILDENV.2016.12.019.

[12]   X. Zhang, A.U. Weerasuriya, J. Wang, C.Y. Li, Z. Chen, K.T. Tse, J. Hang, Cross-ventilation of a generic building with various configurations of external and internal openings, Build Environ. 207 (2022). https://doi.org/10.1016/J.BUILDENV.2021.108447.

[13]   Y. Tominaga, B. Blocken, Wind tunnel experiments on cross-ventilation flow of a generic building with contaminant dispersion in unsheltered and sheltered conditions, Build Environ. 92 (2015) 452–461. https://doi.org/10.1016/J.BUILDENV.2015.05.026.

[14]   N. Ikegaya, S. Hasegawa, A. Hagishima, Time-resolved particle image velocimetry for cross-ventilation flow of generic block sheltered by urban-like block arrays, Build Environ. 147 (2019) 132–145. https://doi.org/10.1016/J.BUILDENV.2018.10.015.

[15]   Y. Adachi, N. Ikegaya, H. Satonaka, A. Hagishima, Numerical simulation for cross-ventilation flow of generic block sheltered by urban-like block array, Build Environ. 185 (2020) 107174. https://doi.org/10.1016/J.BUILDENV.2020.107174.

[16]   C. Hirose, N. Ikegaya, A. Hagishima, J. Tanimoto, Indoor airflow and thermal comfort in a cross-ventilated building within an urban-like block array using large-eddy simulations, Build Environ. 196 (2021). https://doi.org/10.1016/J.BUILDENV.2021.107811.

[17]   K. Kosutova, T. van Hooff, C. Vanderwel, B. Blocken, J. Hensen, Cross-ventilation in a generic isolated building equipped with louvers: Wind-tunnel experiments and CFD simulations, Build Environ. 154 (2019) 263–280. https://doi.org/10.1016/J.BUILDENV.2019.03.019.

[18]   T. Kobayashi, T. Chikamoto, K. Osada, Evaluation of ventilation performance of monitor roof in residential area based on simplified estimation and CFD analysis, Build Environ. 63 (2013) 20–30. https://doi.org/10.1016/J.BUILDENV.2013.01.018.

[19]   Y. Arinami, S. ichi Akabayashi, Y. Tominaga, J. Sakaguchi, Performance evaluation of single-sided natural ventilation for generic building using large-eddy simulations: Effect of guide vanes and adjacent obstacles, Build Environ. 154 (2019) 68–80. https://doi.org/10.1016/J.BUILDENV.2019.01.021.

[20]   Y. Jiang, Q. Chen, Effect of fluctuating wind direction on cross natural ventilation in buildings from large eddy simulation, Build Environ. 37 (2002) 379–386. https://doi.org/10.1016/S0360-1323(01)00036-1.

[21]   H.B. Awbi, Ventilation of buildings: Second edition, Second Edition, Spon Press, London, 2003. https://doi.org/10.4324/9780203634479.

[22]   Y. Li, P. Heiselberg, Analysis Methods for Natural and Hybrid Ventilation - a Critical Literature Review and Recent Developments, International Journal of Ventilation . 1 (2003) 3–20. https://doi.org/10.1080/14733315.2003.11683640.

[23]   P. Heiselberg, M. Sandberg, Evaluation of Discharge Coefficients for Window Openings in Wind Driven Natural Ventilation, International Journal of Ventilation. 5 (2006) 43–52. https://doi.org/10.1080/14733315.2006.11683723.

[24]   P. Karava, T. Stathopoulos, A.K. Athienitis, Wind Driven Flow through Openings – A Review of Discharge Coefficients, International Journal of Ventilation. 3 (2004) 255–266. https://doi.org/10.1080/14733315.2004.11683920.

[25]   J.J. True, M. Sandberg, P. Heiselberg, P. v. Nielsen, Wind Driven Cross-Flow Analysed as a Catchment Problem and as a Pressure Driven Flow, International Journal of Ventilation. 1 (2003) 89–101. https://doi.org/10.1080/14733315.2003.11683647.

[26]   T. Kobayashi, K. Sagara, T. Yamanaka, H. Kotani, S. Takeda, M. Sandberg, Stream Tube based Analysis of Problems in Prediction of Cross-Ventilation Rate, International Journal of Ventilation. 7 (2009) 321–334. https://doi.org/10.1080/14733315.2009.11683822.

[27]   Guffy S.E., Fraser D. A., A power balance model of converging and diverging flow junctions, ASHRAE Trans. 95 (1989) 2–9.

[28]   Murakami S., Kato S., Akabashi S., Mizutani K., Kim Y. D., Wind tunnel test on velocityepressure field of cross-ventilation with open windows, ASHRAE Trans. 97 (1991) 525–538.

[29]   S. Kato, Flow Network Model based on Power Balance as Applied to Cross-Ventilation, International Journal of Ventilation. 2 (2004) 395–408. https://doi.org/10.1080/14733315.2004.11683681.

[30]   W. Axley James, C.H. Daniel, J.W. Axley, D.H. Chung, POWBAM0 Mechanical Power Balances for Multi-zone Building Airflow Analysis, International Journal of Ventilation. 4 (2005) 95–112.

[31]   T. Kobayashi, K. Sagara, T. Yamanaka, H. Kotani, M. Sandberg, Wind Driven Flow Through Openings - Analysis of the Stream Tube, International Journal of Ventilation. 4 (2006) 323–336. https://doi.org/10.1080/14733315.2005.11683712.

[32]   T. Kobayashi, K. Sagara, T. Yamanaka, H. Kotani, M. Sandberg, Power transportation inside stream tube of cross-ventilated simple shaped model and pitched roof house, Build Environ. 44 (2009) 1440–1451. https://doi.org/10.1016/J.BUILDENV.2008.09.013.

[33]   M. Sandberg, An Alternative View on the Theory of Cross-Ventilation, International Journal of Ventilation. 2

(2004) 409–418. https://doi.org/10.1080/14733315.2004.11683682.

[34]   T. Kurabuchi, M. Ohba, T. Endo, Y. Akamine, F. Nakayama, Local Dynamic Similarity Model of Cross-Ventilation Part 1 - Theoretical Framework, International Journal of Ventilation. 2 (2004) 371–382. https://doi.org/10.1080/14733315.2004.11683679.

[35]   M. Ohba, T. Kurabuchi, E. Tomoyuki, Y. Akamine, M. Kamata, A. Kurahashi, Local Dynamic Similarity Model of Cross-Ventilation Part 2 - Application of Local Dynamic Similarity Model, International Journal of Ventilation. 2 (2004) 383–394. https://doi.org/10.1080/14733315.2004.11683680.

[36]   T. Endo, T. Kurabuchi, M. Ohba, Y. Akamine, M. Kamata, A Fundamental Study on the Air Flow Structure of Outflow Openings, International Journal of Ventilation. 2 (2004) 439–446. https://doi.org/10.1080/14733315.2004.11683685.

[37]   T. Kurabuchi, M. Ohba, T. Nonaka, Domain Decomposition Technique Applied to the Evaluation of Cross-Ventilation Performance of Opening Positions of a Building, International Journal of Ventilation. 8 (2009) 207–217. https://doi.org/10.1080/14733315.2009.11683846.

[38]   K. Tsuruta, T. Kurabuchi, Y. Kouchi, Domain Decomposition Technique Applied to the Evaluation of Cross–Ventilation Performance for Various Opening Conditions of a Building, International Journal of Ventilation. 10 (2011) 147–154. https://doi.org/10.1080/14733315.2011.11683943.

[39]   H. Kotani, T. Yamanaka, Flow Visualization and Inflow Direction Measurement at a Cross-Ventilated Large Opening, International Journal of Ventilation. 5 (2006) 79–87. https://doi.org/10.1080/14733315.2006.11683726.

[40]   H. Kotani, T. Yamanaka, Prediction of Inflow Direction at Large Opening of Cross-Ventilated Apartment Building, Journal of Environmental Engineering (Transactions of AIJ). 71 (2006) 39–45. https://doi.org/10.3130/AIJE.71.39_7.

[41]   C. Allocca, Q. Chen, L.R. Glicksman, Design analysis of single-sided natural ventilation, Energy Build. 35 (2003) 785–795. https://doi.org/10.1016/S0378-7788(02)00239-6.

[42]   N.C. Daish, G. Carrilho da Graça, P.F. Linden, D. Banks, Impact of aperture separation on wind-driven single-sided natural ventilation, Build Environ. 108 (2016) 122–134. https://doi.org/10.1016/J.BUILDENV.2016.08.015.

[43]   G. Carrilho da Graça, A technical note on simplified modeling of turbulent mixing in wind-driven single sided ventilation, Build Environ. 131 (2018) 12–15. https://doi.org/10.1016/J.BUILDENV.2018.01.014.

[44]   H.Y. Zhong, Y. Sun, J. Shang, F.P. Qian, F.Y. Zhao, H. Kikumoto, C. Jimenez-Bescos, X. Liu, Single-sided natural ventilation in buildings: a critical literature review, Build Environ. 212 (2022) 108797. https://doi.org/10.1016/J.BUILDENV.2022.108797.

[45]   Malinowski H.K, Wind effect on the air movement inside buildings, Proceedings of 3rd International Conference on Wind Effects on Buildings and Structures, Tokyo. (1971) 125–134.

[46]   J.P. Cockroft, P. Robertson, Ventilation of an enclosure through a single opening, Build Environ. 11 (1976) 29–35. https://doi.org/10.1016/0360-1323(76)90016-0.

[47]   F. Haghighat, J. Rao, P. Fazio, The influence of turbulent wind on air change rates—a modelling approach, Build Environ. 26 (1991) 95–109. https://doi.org/10.1016/0360-1323(91)90017-6.

[48]   F. Haghighat, H. Brohus, J. Rao, Modelling air infiltration due to wind fluctuations—a review, Build Environ. 35 (2000) 377–385. https://doi.org/10.1016/S0360-1323(99)00028-1.

[49]   Warren P. R., Ventilation through openings on one wall only, Energy Conservation in Heating, Cooling, and Ventilating Building. 1 (1978) 189–206.

[50]   Yamanaka Toshio, Narasaki Masaya, Satoh Ryuji, Iwamoto Kiyotaka, Wind-forced ventilation of the room with a single opening - Ventilation based on mixing layer caused by the airflow along opening plane -, Transactions of AIJ. Journal of Architecture, Planning and Environmental Engineering (In Japanese). 64 (1999) 37–43. https://doi.org/10.3130/AIJA.64.37_1.

[51]   T. Yamanaka, H. Kotani, K. Iwamoto, M. Kato, Natural, wind-forced ventilation caused by turbulence in a room with a single opening, International Journal of Ventilation. 5 (2006) 179–187.

https://doi.org/10.1080/14733315.2006.11683735.

[52]   S. Kato, R. Kono, T. Hasama, R. Ooka, T. Takahashi, A wind tunnel experimental analysis of the ventilation characteristics of a room with single-sided opening in uniform flow, International Journal of Ventilation. 5 (2006) 171–178. https://doi.org/10.1080/14733315.2006.11683734.

[53]   T. Hasama, S. Kato, R. Ooka, Analysis of wind-induced inflow and outflow through a single opening using LES & DES, Journal of Wind Engineering and Industrial Aerodynamics. 96 (2008) 1678–1691. https://doi.org/10.1016/J.JWEIA.2008.02.005.

[54]   T.S. Larsen, P. Heiselberg, Single-sided natural ventilation driven by wind pressure and temperature difference, Energy Build. 40 (2008) 1031–1040. https://doi.org/10.1016/J.ENBUILD.2006.07.012.

[55]   C.R. Chu, R.H. Chen, J.W. Chen, A laboratory experiment of shear-induced natural ventilation, Energy Build. 43 (2011) 2631–2637. https://doi.org/10.1016/J.ENBUILD.2011.06.014.

[56]   H. Wang, Q. Chen, A new empirical model for predicting single-sided, wind-driven natural ventilation in buildings, Energy Build. 54 (2012) 386–394. https://doi.org/10.1016/J.ENBUILD.2012.07.028.

[57]   M. Caciolo, P. Stabat, D. Marchio, Numerical simulation of single-sided ventilation using RANS and LES and comparison with full-scale experiments, Build Environ. 50 (2012) 202–213. https://doi.org/10.1016/J.BUILDENV.2011.10.017.

[58]   Z. Bu U, S. Kato, Wind-induced ventilation performances and airflow characteristics in an areaway-attached basement with a single-sided opening, Build Environ. 46 (2011) 911–921. https://doi.org/10.1016/J.BUILDENV.2010.10.019.

[59]   A. Hayati, M. Mattsson, M. Sandberg, A wind tunnel study of wind-driven airing through open doors, International Journal of Ventilation. 18 (2019) 113–135. https://doi.org/10.1080/14733315.2018.1435027.

[60]   Z.T. Ai, C.M. Mak, Analysis of fluctuating characteristics of wind-induced airflow through a single opening using LES modeling and the tracer gas technique, Build Environ. 80 (2014) 249–258. https://doi.org/10.1016/J.BUILDENV.2014.06.002.

[61]   H. Wang, Q. Chen, Modeling of the Impact of different Window Types on Single-sided Natural Ventilation, Energy Procedia. 78 (2015) 1549–1555. https://doi.org/10.1016/J.EGYPRO.2015.11.201.

[62]   C.R. Chu, Y.H. Chiu, Y.T. Tsai, S.L. Wu, Wind-driven natural ventilation for buildings with two openings on the same external wall, Energy Build. 108 (2015) 365–372. https://doi.org/10.1016/J.ENBUILD.2015.09.041.

[63]   G. Carrilho da Graça, P. Linden, Ten questions about natural ventilation of non-domestic buildings, Build Environ. 107 (2016) 263–273. https://doi.org/10.1016/J.BUILDENV.2016.08.007.

[64]   D.P. Albuquerque, M. Sandberg, P.F. Linden, G. Carrilho da Graça, Experimental and numerical investigation of pumping ventilation on the leeward side of a cubic building, Build Environ. 179 (2020) 106897. https://doi.org/10.1016/J.BUILDENV.2020.106897.

[65]   H.Y. Zhong, C. Lin, Y. Sun, H. Kikumoto, R. Ooka, H.L. Zhang, H. Hu, F.Y. Zhao, C. Jimenez-Bescos, Boundary layer wind tunnel modeling experiments on pumping ventilation through a three-story reduce-scaled building with two openings, Build Environ. 202 (2021) 108043. https://doi.org/10.1016/J.BUILDENV.2021.108043.

[66]   G. Carrilho da Graça, D.P. Albuquerque, M. Sandberg, P.F. Linden, Pumping ventilation of corner and single sided rooms with two openings, Build Environ. 205 (2021) 108171. https://doi.org/10.1016/J.BUILDENV.2021.108171.

[67]   Z. Jiang, T. Kobayashi, T. Yamanaka, M. Sandberg, N. Kobayashi, N. Choi, K. Sano, Validity of Orifice equation and impact of building parameters on wind-induced natural ventilation rates with minute mean wind pressure difference, Build Environ. 219 (2022) 109248. https://doi.org/10.1016/J.BUILDENV.2022.109248.

[68]   D. W. Etheridge, M. Sandberg, Building ventilation: theory and measurement, John Wiley & Sons, 1996.

[69]   ISO 12569:2017, Thermal performance of buildings and materials — Determination of specific airflow rate in buildings — Tracer gas dilution method, (2017). https://www.iso.org/standard/69817.html.

[70]   A. Smirnov, S. Shi, I. Celik, Random Flow Generation Technique for Large Eddy Simulations and Particle-

Dynamics Modeling, J Fluids Eng. 123 (2001) 359–371. https://doi.org/10.1115/1.1369598.

[71]   S.A. Morsi, A.J. Alexander, An investigation of particle trajectories in two-phase flow systems, J Fluid Mech. 55 (1972) 193–208. https://doi.org/10.1017/S0022112072001806.

Turbulence Model		Large Eddy Simulation Smagorinsky-Lilly Model (C_s=1.0)	
CFD Code		Ansys Fluent 17.0	
Algorithm		Implicit method (SIMPLE)	
Discretization Scheme for Advection Term		Central Differencing	
Boundary Condition	Inlet	Based on wind tunnel measurement and Smirnov's method	
	Outlet	Gauge Pressure : 0 [Pa]	
	Walls	Two Layer Model of Linear-Log Law	
Model		Sealed Model	Opening Model
Time Step		0.0001 [s]	0.0005 [s]
Preconditioning Calculation Term		10,000 time step (=1.0 [s])	2,000 time step (=1.0 [s])
Main Calculation Term		100,000 time step (=10 [s])	20,000 time step (=10 [s])
Total Number of Cells		19,66,720	1,753,350 (Case 1)
			1,192,100 (Case 2)
			1,753,350 (Case 3)

Description	Case ID	Central Position of Opening (X, Y, Z) [mm]		Cp and mean velocity in its vicinity				ΔCp [-]	σ_ΔCp [-]	AFR [L/min]	PFR [L/min]	PFR/AFR [%]
				Opening 1		Opening 2						
		Opening 1	Opening 2	Cp [-]	Vvic [m/s]	Cp [-]	Vvic [m/s]					
	DS 0-0	L=100 (0, 100, -100)	R=100 (0, 100, 100)	-0.73	1.41	-0.74	1.39	0.007	0.236	112.1	88.1	78.59
	DS 0-1	L=80 (-20, 100, -100)	R=80 (-20, 100, 100)	-0.81	1.47	-0.82	1.48	0.012	0.221	99.8	74.8	75.03
	DS 0-2	L=60 (-40, 100, -100)	R=60 (-40, 100, 100)	-0.83	1.31	-0.84	1.33	0.007	0.201	88.9	62.1	69.78
	DS 0-3	L=120 (20, 100, -100)	R=120 (20, 100, 100)	-0.63	1.23	-0.63	1.15	0.001	0.244	123.0	96.8	78.67
	DS 0-4	L=140 (40, 100, -100)	R=140 (40, 100, 100)	-0.52	0.85	-0.51	0.81	0.010	0.247	135.0	106.8	79.08
	DS 1	L=80 (-20, 100, -100)	R=100 (0, 100, 100)	-0.81	1.47	-0.74	1.39	0.065	0.229	111.7	78.0	69.84
	DS 2	L=80 (-20, 100, -100)	R=40 (-60, 100, 100)	-0.81	1.47	-0.81	1.11	0.003	0.206	95.4	67.5	70.83
	DS 3	L=80 (-20, 100, -100)	R=120 (20, 100, 100)	-0.81	1.47	-0.63	1.15	0.173	0.237	124.6	89.5	71.77
	DS 4	L=80 (-20, 100, -100)	R=130 (30, 100, 100)	-0.81	1.47	-0.57	0.99	0.236	0.237	134.6	98.1	72.89
	DS 5	L=80 (-20, 100, -100)	R=140 (40, 100, 100)	-0.81	1.47	-0.51	0.81	0.299	0.234	149.6	115.9	77.49
	SS-L1	L_1=100 (0, 100, -100)	L_2=50 (-50, 100, -100)	-0.73	1.41	-0.82	1.18	0.089	0.235	95.8	58.0	60.51
	SS-L2	L_1=100 (0, 100, -100)	L_2=40 (-60, 100, -100)	-0.73	1.41	-0.80	1.16	0.065	0.218	98.9	61.2	61.82
	SS-L3	L_1=100 (0, 100, -100)	L_2=30 (-70, 100, -100)	-0.73	1.41	-0.77	1.37	0.040	0.199	100.5	62.1	61.77
	SS-F1	F_1=30 (-100, 100, -30)	F_2=30 (-100, 100, 30)	0.62	2.13	0.62	2.13	0.001	0.048	80.9	76.2	94.16
	SS-F2	F_1=40 (-100 ,100, -40)	F_2=40 (-100, 100, 40)	0.61	2.29	0.61	2.28	0.002	0.061	86.2	80.8	93.66
	SS-F3	F_1=50 (-100, 100, -50)	F_2=50 (-100, 100, 50)	0.59	2.49	0.59	2.47	0.003	0.071	90.3	80.3	88.97
	SS-B1	B_1=(100, 100, -30)	B_2=30 (100, 100, 30)	-0.23	1.17	-0.23	1.25	0.002	0.057	56.4	52.0	92.20
	SS-B2	B_1=(100, 100, -40)	B_2=40 (100, 100, 40)	-0.24	1.26	-0.24	1.34	0.001	0.068	60.0	55.7	92.83
	SS-B3	B_1=(100, 100, -50)	B_2=50 (100, 100, 50)	-0.24	1.33	-0.24	1.37	0.000	0.078	64.8	55.7	85.92

Highlights

- Wind-induced natural ventilation under small wind pressure difference was analysed
- Orifice equation failed largely if pressure coefficient difference is less than 0.065
- Ratio of effective to bulk airflow rate was analysed as ventilation efficiency
- Ventilation efficiency under no wind pressure difference depends on opening position
- Flow rate cannot be determined by only wind pressure difference and its deviation

September 30th, 2022

Title: "Numerical analysis of wind-induced natural ventilation for an isolated cubic room with two openings under small mean wind pressure difference"

Conflict of interest disclosure
The authors declare no conflicts of interest associated with this manuscript.

Tomohiro KOBAYASHI
Osaka University
2-1 Yamadaoka, Suita, Osaka, JAPAN Zip 565-0871 +81-6-6879-7644
+81-6-6879-7646 (FAX) kobayashi@arch.eng.osaka-u.ac.jp